

A Filament-Associated Halo Coronal Mass Ejection

Jun Zhang¹ *, Jingxiu Wang¹, and Nariaki Nitta²

¹ Beijing Astronomical Observatory, National Astronomical Observatories,
Chinese Academy of Sciences, Beijing 100012

² Lockheed Martin Solar and Astrophysics Laboratory, Palo Alto, CA 94304, USA

Received 2000 November 14; accepted 2001 January 3

Abstract There are only a few observations published so far that show the initiation of a coronal mass ejection (CME) and illustrate the magnetic changes in the surface origin of a CME. Any attempt to connect a CME with its local solar activities is meaningful. In this paper we present a clear instance of a halo CME initiation. A careful analysis of magnetograms shows that the only obvious magnetic changes in the surface region of the CME is a magnetic flux cancellation underneath a quiescent filament. The early disturbance was seen as the slow upward motion in segments of the quiescent filament. Four hours later, the filament was accelerated to about 50 km s^{-1} and erupted. While a small part of the material in the filament was ejected into the upper corona, most of the mass was transported to a nearby region. About forty minutes later, the transported mass was also ejected partially to the upper corona. The eruption of the filament triggered a two-ribbon flare, with post-flare loops connecting the flare ribbons. A halo CME, which is inferred to be associated with the eruptive filament, was observed from LASCO/C2 and C3. The halo CME contained two CME events, each event corresponded to a partial mass ejection of the filament. We suggest that the magnetic reconnection at the lower atmosphere is responsible for the filament eruption and the halo CME.

Key words: Sun: filament — Sun: magnetic fields — Sun: coronal mass ejection

1 INTRODUCTION

Coronal mass ejections (CMEs) are often seen as spectacular eruptions of matter from the Sun which propagate outward through the heliosphere and often interact with the Earth's magnetosphere (Hundhausen, 1997; Gosling, 1997; and references herein). It is well known that these interactions can have substantial consequences on the geomagnetic environment of the Earth, sometimes resulting in damage to satellites (e.g., McAllister et al., 1996; Berdichevsky et al., 1998). CMEs have been often described as a three-part structure consisting of a bright loop overlying a coronal cavity containing a bright core of denser material coming from an eruptive prominence (Illing and Hundhausen, 1985). Dere et al. (1997) presented an excellent observation of all 3 components of a CME.

* E-mail: zjun@ourstar.bao.ac.cn

CMEs are often associated with prominence eruptions and/or solar flares (see Zhang and Wang, 2000). However, the nature and cause of CMEs is an unsolved, fundamental problem in solar physics. In particular, the CMEs that are easiest to see with coronagraphs are those that are in the plane of the sky. Thus, the most readily visible CMEs originate preferentially from the limb of the Sun. Low-altitude coronal source regions of these CMEs would often be seen in projection at the limb, thereby precluding clear views of the coronal features responsible for the eruptions. Halo CMEs, which originate from the disk, are earth-directed mass ejections. The first halo CME was reported by Howard et al. (1982), using observations made with the Solwind coronagraph on the P78-1 spacecraft. Several halo-CME events have been reported by LASCO (Plunkett et al., 1998; Thompson et al., 1998). The study on halo CMEs would help us to establish a correlation between disk active phenomena and limb CMEs, to understand their ejection mechanism and, eventually, to forecast when the eruptions will occur.

The eruption of a filament usually triggers a flare. Post-flare loop systems appear frequently as a development of large, two-ribbon eruptive flares (Bray et al., 1991; Švestka and Cliver, 1992) and have been explained by models of reconnection of magnetic field lines in the high corona with an X -point where plasma is strongly heated. The reconnection of magnetic fields is the basic ingredient of the solar flare mechanism (Bruzek, 1964). According to the basic reconnection flare model (RFM), hot loops with temperatures of $\sim 3 \times 10^7$ K form soon after the flare onset. These loops are essentially magnetic flux tubes filled with hot plasma. The regions joined by these loops are brightened due to heating by thermal conduction, shocks, and/or non-thermal particles generated in the reconnection process. The two-ribbon flares with post-flare loop activity are believed to be classical examples of the RFM (Choudhary and Gary, 1999). Continuous reconnection of open or greatly elongated field lines takes place at the magnetic X -line which moves upward (Carmichael 1964, Sturrock 1966, Hirayama 1974, Kopp and Pneuman 1976, Forbes et al. 1989). Heat conducted along field lines mapping from the reconnection region to the chromosphere ablates chromospheric plasma and creates associated flare ribbons. In this paper we present the whole process of a solar event on June 24, 1999. The solar event include (1) the eruption of a quiescent filament; (2) the appearance of a two-ribbon flare and of post-flare loops; and (3) a halo CME. We also suggest that the magnetic reconnection at the lower atmosphere triggered the solar event.

The *Solar and Heliospheric Observatory* (SOHO) has provided unprecedented observations of the Sun and the heliosphere. In this paper, we present observations made by 3 of the instruments on SOHO, the Extreme Ultraviolet Imaging Telescope (EIT), the Michelson Doppler Imager (MDI) and the Large Angle Spectrometric Coronagraph (LASCO). A detailed description of these instruments was provided by Delaboudinière et al. (1995), Scherrer et al. (1995) and Brueckner et al. (1995).

2 FILAMENT ERUPTION AND ASSOCIATED MAGNETIC FIELD EVOLUTION

The 1999 June 24 halo CME originated near 30N 15W on the Sun, where a quiescent filament erupted at 13:11 UT. Figure 1 shows the configuration and evolution of the filament (the arrows in the upper two rows), in the two days of June 23 and 24. Left column presents $H\alpha$ filtergrams from Big Bear Solar Observatory (BBSO) (the upper and lower panels) and Observatoire de Paris (the middle panel); right column shows two SOHO EIT images (the upper and lower panels) and an MDI magnetogram (the middle-right panel). Black patches in

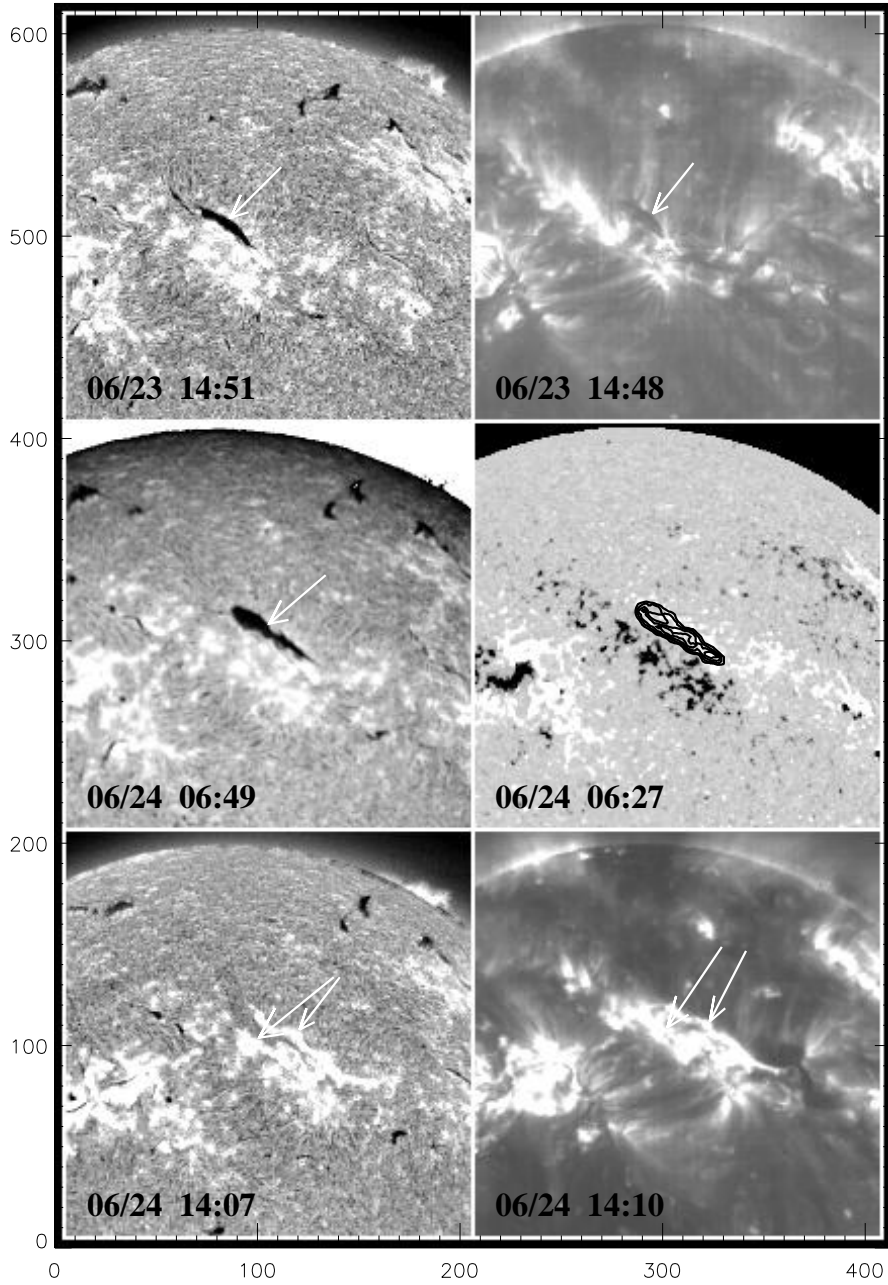


Fig. 1 Three H_{α} central line filtergrams (left column) from Big Bear Solar Observatory (the upper and lower images) and Observatoire de Paris (the middle image), two SOHO EIT images (right column, the upper and lower images), and an MDI magnetogram (right column, the middle panel in the right column) present the disk segments of the filament. The arrows used in this figure are described in the text. 1 unit = 4.97 arcsec.

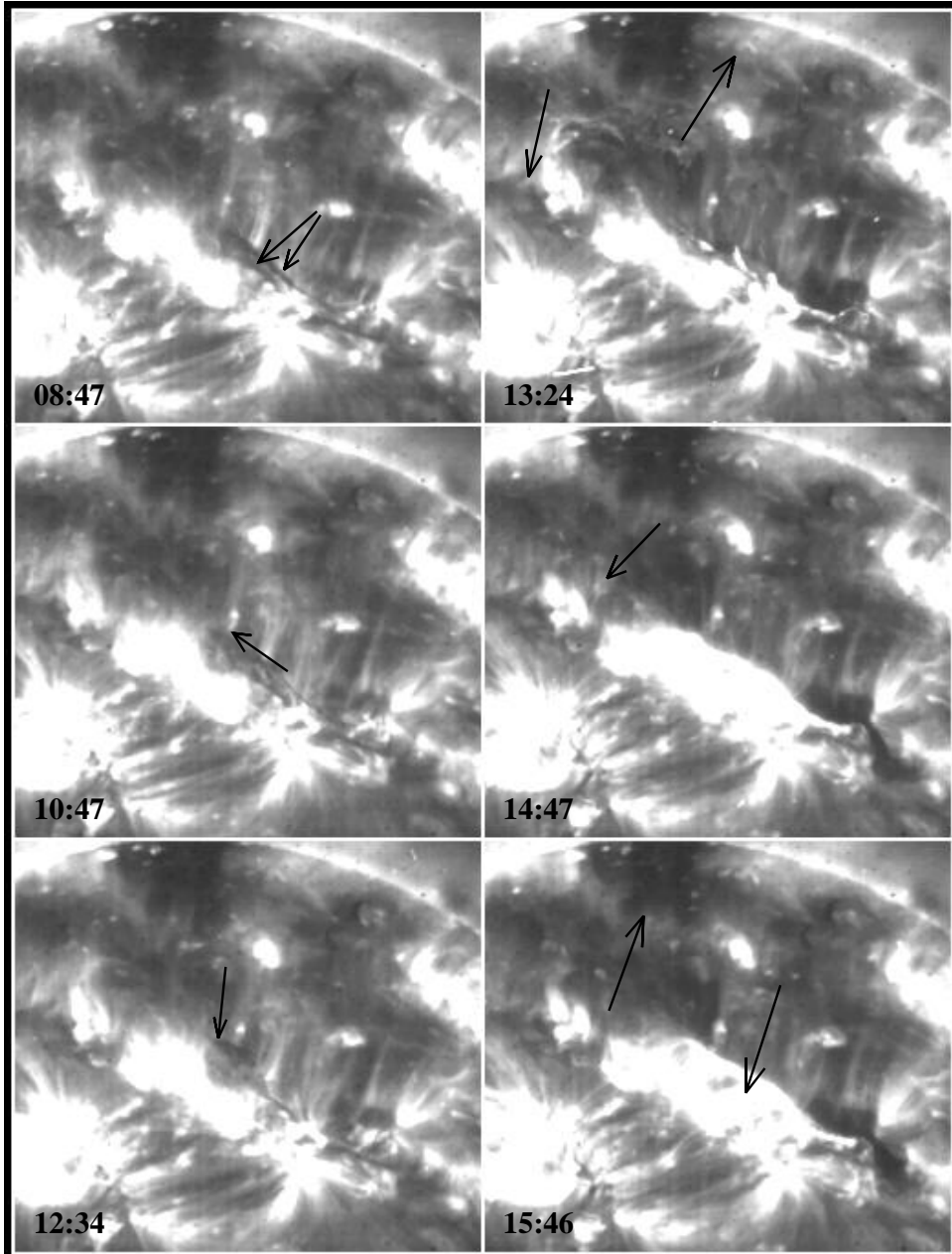


Fig. 2 Time sequence of EIT 195 Å images showing the filament eruption.
The arrows used in this figure are described in the text.

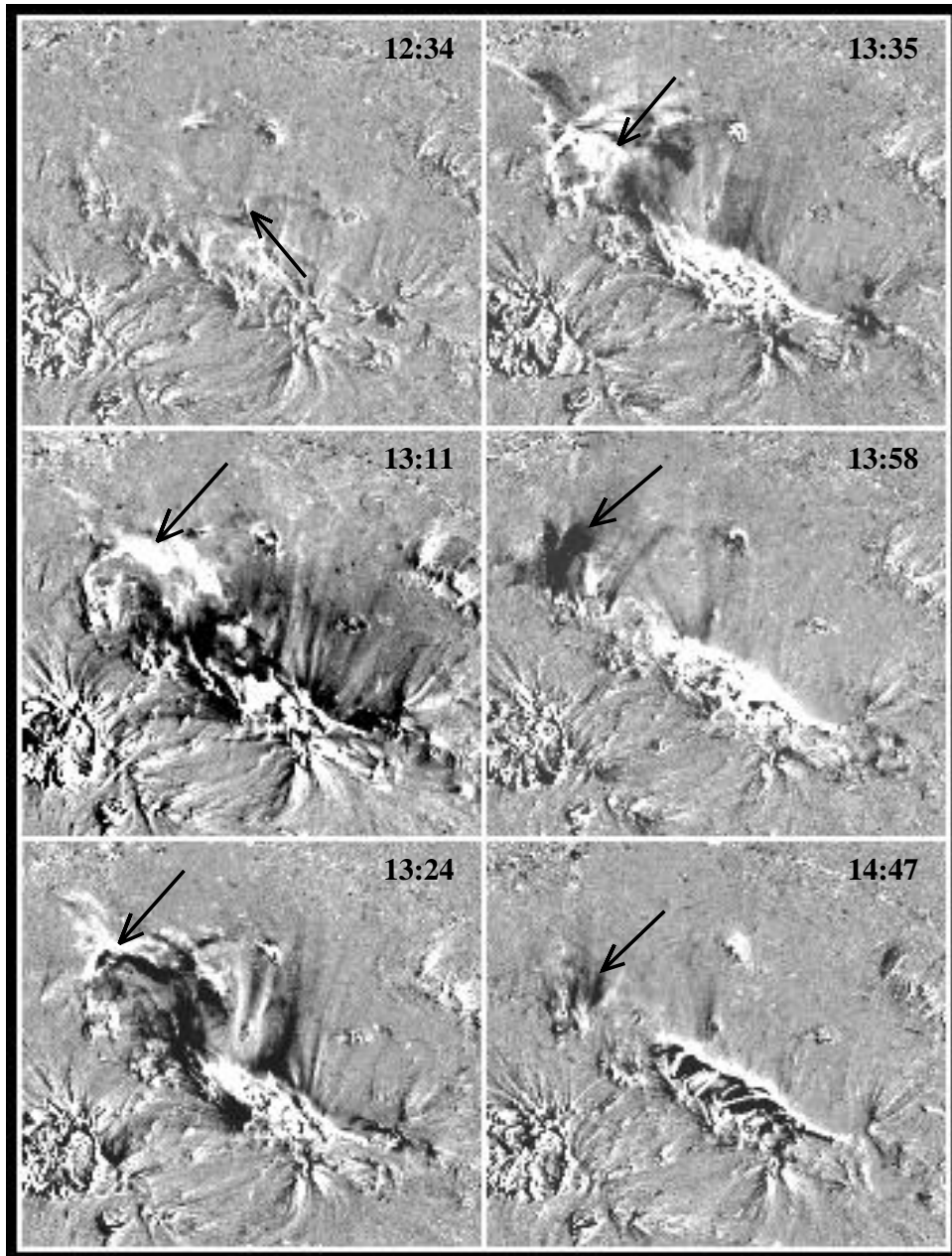


Fig. 3 Running difference of EIT 195Å images showing the filament eruption. The arrows used in this figure are described in the text.

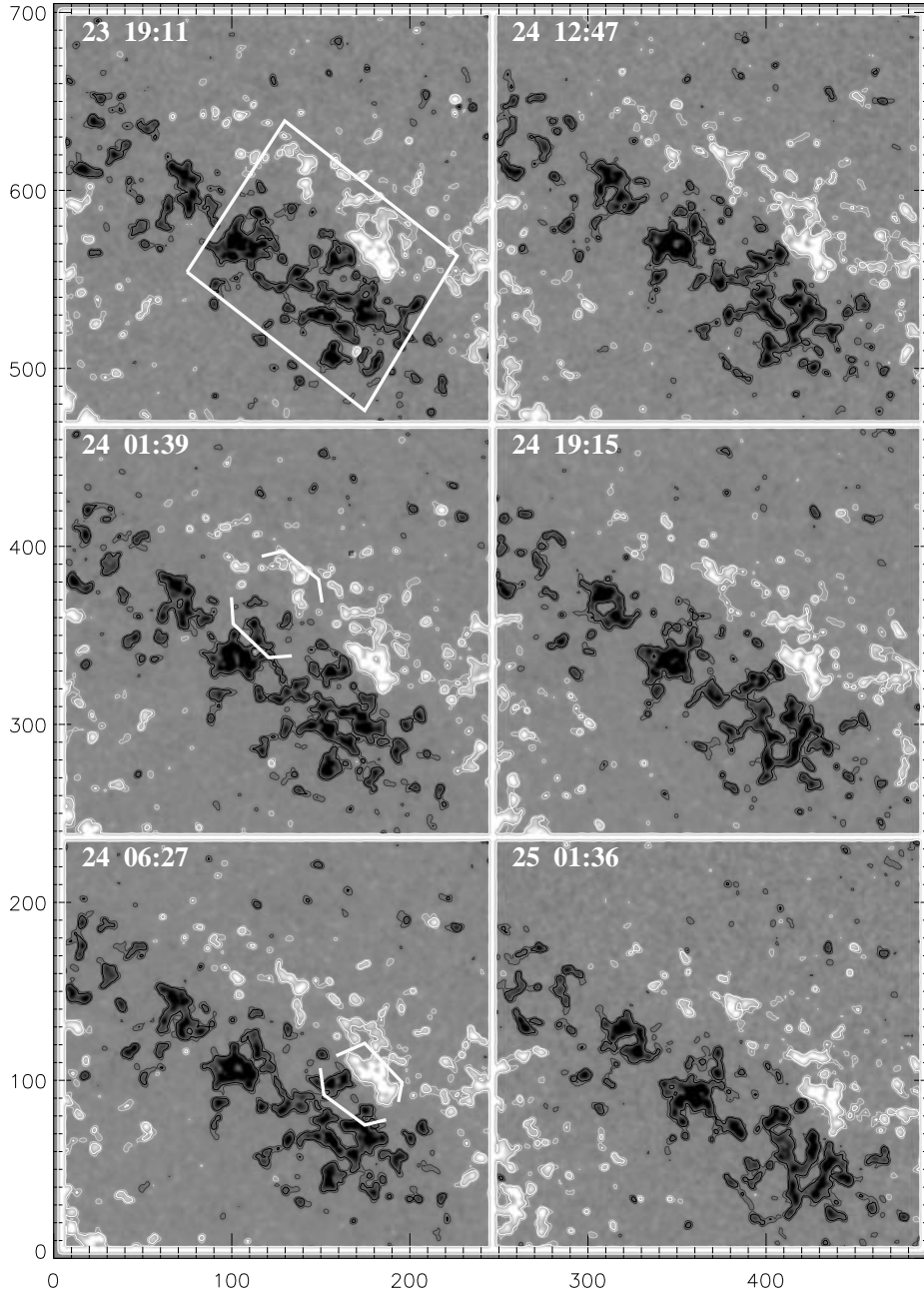


Fig. 4 Time sequence of line-of-sight magnetograms from SOHO MDI. White patches present positive polarity fields, and black patches, negative polarity fields. Contour levels are ± 20 and 40 G. The window and square brackets in this figure are described in the text. The field of view is about 480 by 460 square arcsec.

the MDI magnetogram represent negative magnetic fields, and white patches, positive magnetic fields. From the MDI magnetogram, we found the filament (shown by thick lines) to be located on the neutral line of opposite polarity magnetic fields. The eruption of the filament triggered a two-ribbon flare (the arrows in the lower row), with post-flare loop connecting the ribbons.

Detailed erupting process of the filament was illustrated by the time sequence of EIT 195 Å images in Figures 2 and 3. The filament consisted of two threads (shown by the two arrows at 08:47 UT). At first, the upper thread was disturbed, there was a directed motion of the material in the thread. The arrow at 10:47 UT shows the direction of motion. It seems that the filament material was piled up at one end (the arrow at 12:34 UT) before its eruption. After undergoing several hours of disturbance, the filament finally erupted at 13:11 UT. A small part of the material in the filament was ejected into the upper corona, the right arrow at 13:24 UT shows the direction of the mass ejection. However, the major part of the material was transported to a nearby region and fell towards the lower corona (shown by the left arrow at 13:24 UT). Moreover, the filament material became emission features during its eruption. From the EIT movie, we found that partial falling mass suddenly ejected again into the upper corona, e.g., the filament mass shown by the arrow at 14:47 UT ejected upwards before 15:46 UT. The left arrow at 15:46 UT shows the direction of the ejection. A two-ribbon flare was triggered by the filament eruption, as can be seen from the H α filtergram and EIT images (see Figure 1). The flare ribbons were connected by post-flare loops (shown by a right arrow at 15:46 UT).

The weak coronal emissions associated with the filament eruption was best shown by the EIT running difference images in Figure 3. Each image had the previous image subtracted from it. This method of displaying the images was chosen since it is best at showing faint features. The arrow at 12:34 UT shows the direction of motion of the filament material, and the arrows labeled from 12:46 to 13:35 UT show the mass of the eruptive filament. At 13:11 UT, a large dimming area appeared while the whole body of the filament erupted. As Figure 2 showed, the majority of the filament material fell towards the lower corona in the interval from 12:46 to 13:35 UT. Then the mass that once was transported to the nearby region also ejected partially to the upper corona, the two arrows at 13:58 and 14:47 UT show the dimming area which originated from the second mass ejection.

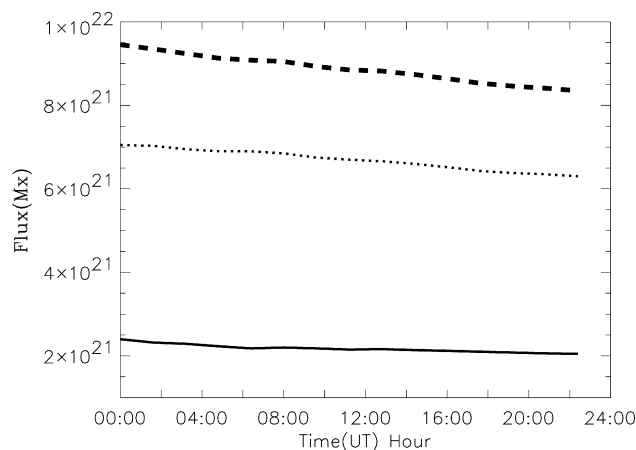


Fig. 5 Magnetic flux in the region shown by the window in Figure 4 as function of time. The dotted, solid and dashed curves indicate the negative, positive and mutual (in both the positive and negative) magnetic flux, respectively.

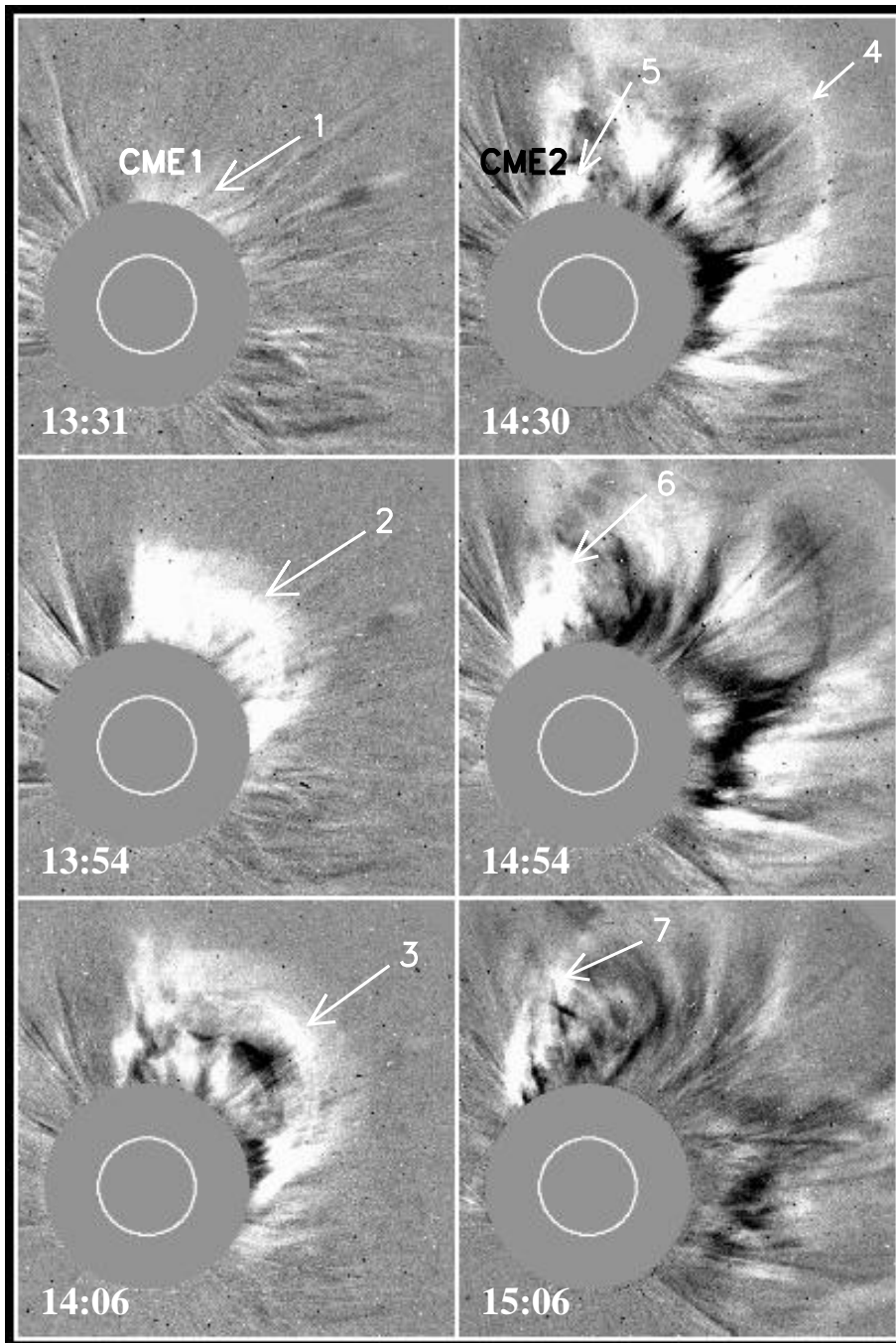


Fig. 6 Running difference of LASCO C2 images on June 24, 1999. The letters and arrows in this figure are described in the text.

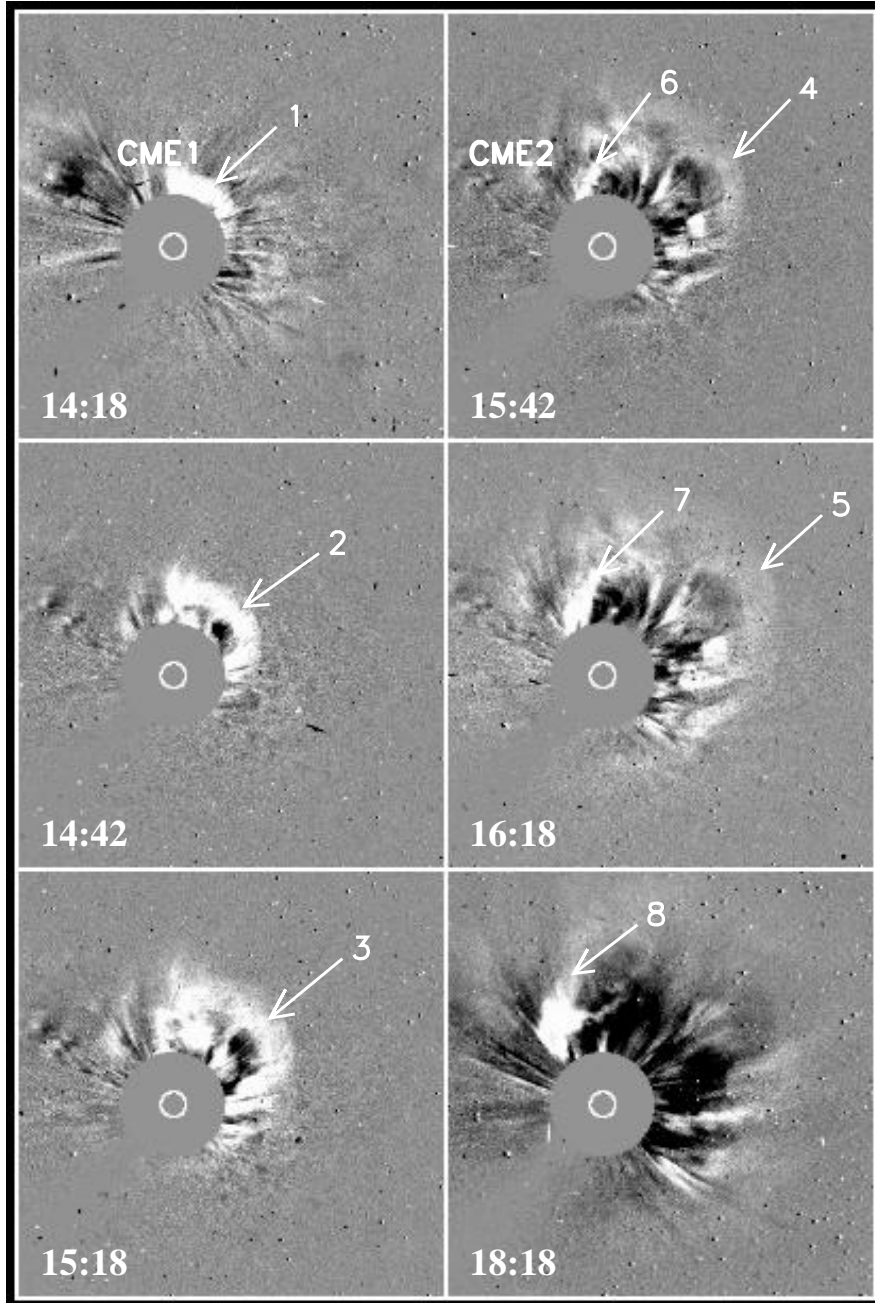


Fig. 7 Running difference of LASCO C3 images on June 24, 1999. The letters and arrows in this figure are described in the text.

To connect the magnetic field configuration with the chromosphere-corona active phenomena, we present the time sequence of line-of-sight magnetograms from SOHO MDI in the region of the eruptive filament in Figure 4. White patches represent positive polarity fields, and black patches, negative fields. Contour levels are ± 20 and 40 G. In this region, violent cancellation of magnetic flux took place below the filament. We have marked the cancellation sites by square brackets at 01:39 and 06:27 UT. In order to show the mutual flux disappearance in the flux cancellation, we present in Figure 5 the temporal evolution of the magnetic flux in the windowed region in Figure 4. The simultaneous decrease in both the positive and negative magnetic flux was about 1.2×10^{21} Mx, in the interval from June 23, 23:59 UT to June 24, 22:27 UT.

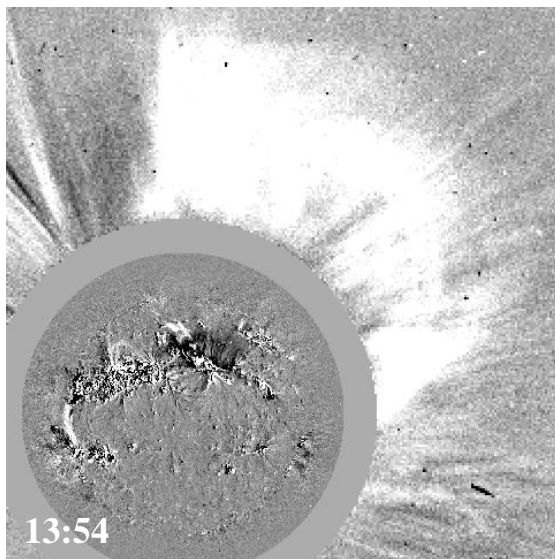


Fig. 8 Composite images of a running difference LASCO C2 13:54 UT image with a running difference EIT 13:11 UT image.

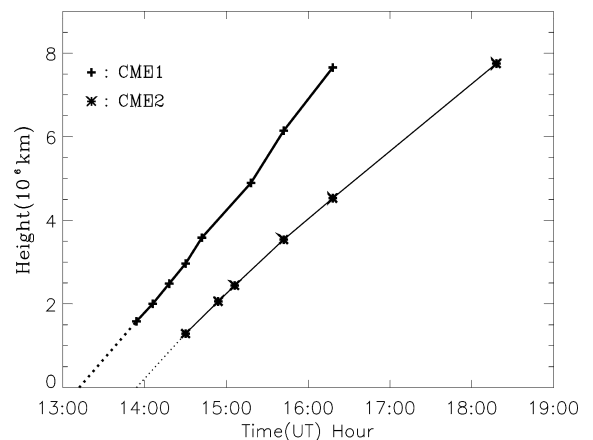


Fig. 9 Height of the leading edges of the two events ‘CME1’ and ‘CME2’ as functions of time.

3 INITIATION OF A HALO CME

The SOHO LASCO observations show that, just after the filament eruption, a wonderful halo CME first appeared in the C2 field of view near 13:31 UT. Figures 6 and 7 display running difference LASCO C2 and C3 images. It looks as though the halo CME contained two CME events, which we label as ‘CME1’ and ‘CME2’. Arrows 1–4 indicate the leading edge of the first event ‘CME1’. The second event ‘CME2’ first appeared at 14:30 UT, and arrows 5–7 mark its leading edge. ‘CME1’ (‘CME2’) first appeared in C3 field of view at 14:18 UT (15:42 UT). Similarly, arrows 1–5 mark the leading edge of ‘CME1’, and arrows 6–8, that of ‘CME2’. By overlaying the EIT and LASCO C2 images with the same spatial scale, we present in Figure 8 a composite sequence of a running difference LASCO C2 13:54 UT image with a running difference EIT 13:11 UT image. The largest EIT dimming area corresponds to ‘CME1’. Hudson and Webb (1997) suggested that coronal dimmings are the remnant signatures of the eruption of large-scale magnetic flux ropes that occurs during CMEs. As the largest dimming

area was associated with the first ejection of the eruptive filament, we deduce that ‘CME1’ was related to the first mass ejection. In order to determine the surface origin of the halo CME, we plot in Figure 9, the heights of the leading edges of the two events ‘CME1’ and ‘CME2’ as functions of time. The values for the heights were determined on assuming that the CMEs were moving radially outward from the center of the region where the filament was located, e.g., the middle part of the filament. ‘CME1’ first clearly appeared in C2 field-of-view at 13:54 UT, then, it appeared in C3 field-of-view at 14:18 UT. ‘CME2’ appeared in C2 (C3) field of view at 14:30 UT (15:42 UT). To decide the surface initiations of the two CME events, we back extrapolated the two curves to the center of the filament region. It was found that, if the CME events were originated from the region, the initial time was near 13:10 UT (13:55 UT) for ‘CME1’ (‘CME2’). Looking at the EIT images, we found that a filament was erupted near 13:11 UT, a minor part of the filament material ejected into the upper corona. And near 13:58 UT, the second mass ejection of the filament took place. For the above reasons, we suggest that the two CME events originate in the filament region and are associated with the two mass ejections of the filament. The whole time sequence of the halo CME initiation is summarized in Figure 10.

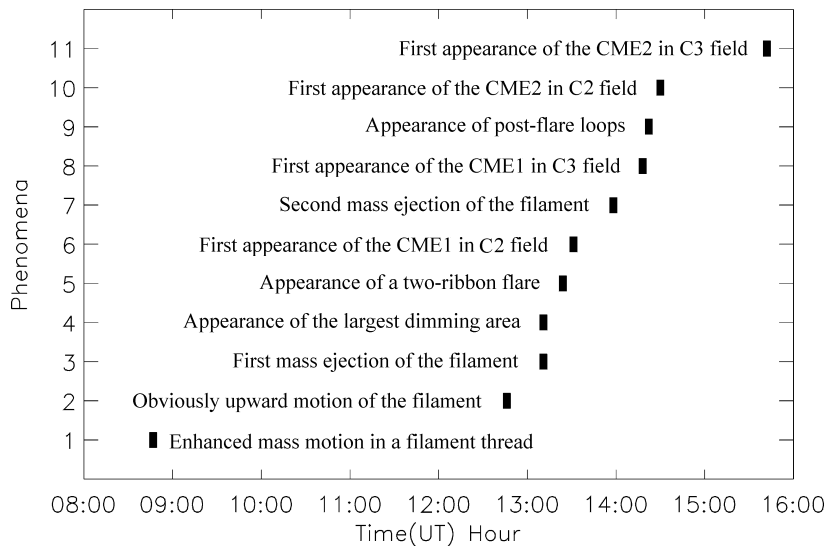


Fig. 10 Diagram of the halo CME initiation. Each vertical bar corresponding to the time that an active phenomenon begins at.

4 RESULTS AND DISCUSSIONS

It was suggested that there is a physical link between cancellation of magnetic field and eruptive flares (Martin and Livi, 1992). The filament magnetic field is a principal site of flare energy storage and magnetic field cancellation represents a direct transfer of magnetic flux, and hence energy, from the photosphere into the filament. Wang and Shi (1993) presented a two-step reconnection scenario for flare energy process. The first-step reconnection takes place in the photosphere, or lower atmosphere, which manifests itself as flux cancellation observed

in the photospheric magnetograms. It is slow but continuous. This slow reconnection may convert the magnetic energy into heat and kinetic energy; but, more important, it can transport magnetic energy and complexity into the rather large-scale magnetic structure higher in the corona. The second-step reconnection, which is explosive in nature and directly responsible for the energy released in transient solar activities, can only take place when some critical status is achieved in the corona (Wang, 2001). The key idea of these authors is to emphasize the overwhelming importance of magnetic reconnection in the lower solar atmosphere in the energetics of explosive solar activities. On the other hand, some observations showed that there are large-scale, magnetic arcades over a filament (Zirin, 1986; Engvold, 1989). These magnetic

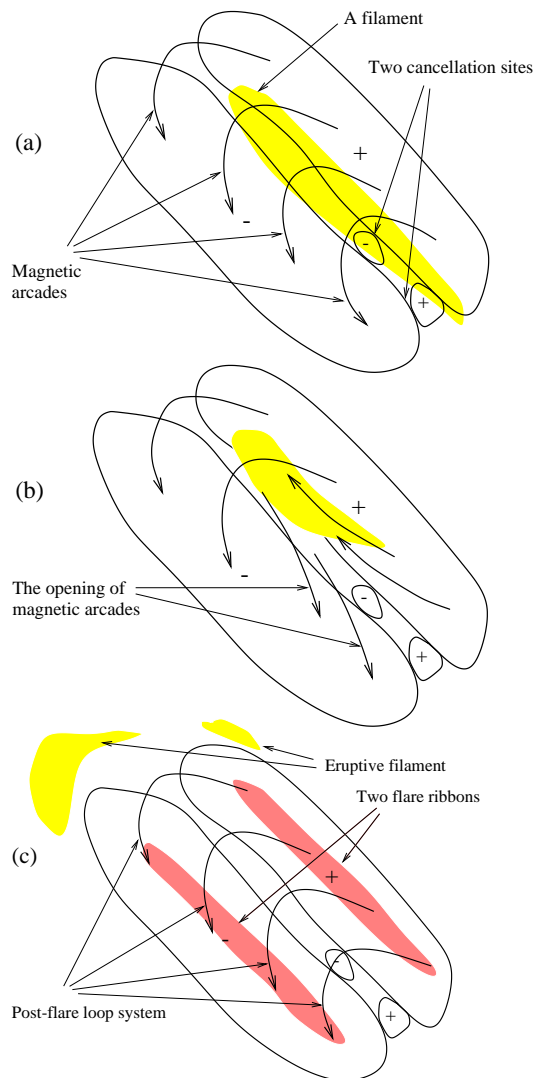


Fig. 11 Carton of the magnetic fields evolution and the associated filament eruption.

arcades might help to restrain the filament from leaving the Sun. When the restraining conditions are altered, filament instability can be taken as a matter of course. We believe that the flux cancellation underneath the filament can gradually change the linkage of a filament to the photosphere and can destabilize the large-scale magnetic arcade enveloping the filament.

The multi-wavelength observations show that the magnetic flux cancellation underneath the filament resulted in the eruption of the filament and the destabilization of the large-scale magnetic arcade which restrained the filament. We suggest that the filament first erupts from regions where the magnetic tension and pressure are weaker. Eruptive filament tears open the pre-existing closed magnetic loop (Kopp and Pneuman, 1976). In addition, magnetic reconnection in the upper corona takes place, and plasma inside the reconnection region is strongly heated. Hot plasma brightens the magnetic loop region by thermal conduction, shocks, and/or non-thermal particles generated in the reconnection process, and thus produces two-ribbon flares with post-flare loop activity (Choudhary and Gary, 1999).

Our morphological findings can be summarized in the schematic diagram of Figure 11. In the disturbance stage of the filament (Fig. 11a), magnetic loops straddle the region between two opposite-polarity regions with their footpoints rooted in these magnetic regions. Meanwhile flux cancellation continuously takes place underneath the filament. Low (1992) has proposed a magnetostatic model to obtain the levitated magnetic ropes interpretable as chromospheric filaments. Van Ballegoijen and Martens (1989) proposed a model of filament formation and eruption. They suggested that flux cancellation interpreted as magnetic reconnection at the neutral line of a sheared magnetic field would lead to the formation of helical field lines which are capable of supporting filament plasma and eventually would lead to filament eruption. We speculate that the flux cancellation underneath the filament causes changes in the configuration of field lines (see Wang, Shi and Martin, 1996) that support the filament. At a critical point, equilibrium of the filament breaks down and the filament erupts (Fig. 11b). The eruptive filament tears open the pre-existing closed magnetic arcade. Since the arcade is either absent or very weak in the eruptive stage, it will appear as a dimmed region (see the image at 13:11 UT in Figure 3). The erupted arcade stretches upward and, two sets of anti-parallel magnetic field lines form and mutually reconnect. The reconnected field lines shrink and become rounded loops. The loops cool to become visible in EUV (see, e.g., Švestka et al. 1987; Forbes and Acton, 1996; Hori et al., 1998) as post-flare loops (Fig. 11c), these loops connect the two-ribbon flare that created in the reconnection process.

Even though the scale of magnetic fields associated with flares, filaments and CMEs is not clear, it is believed that magnetic fields in the corona change their structure substantially after a flare onsets, a filament eruption or a CME event. However, few examples are known that show large scale or local photospheric magnetic field changes during flares and CMEs (Zhang and Wang, 2001; Zhang et al., 2001). In this paper, we show a good example of obvious changes in the line-of-sight magnetic field during a filament eruption and CME event. Magnetic flux cancellations are the most common phenomena of magnetic evolution. Their consequences are eruption of filament, appearance of flares and post-flare loops, and generation of the halo CME.

Acknowledgment This work is supported by the Major Project 19791090, funded by the National Natural Science Foundation of China (NSFC). The authors are indebted to the SOHO EIT, LASCO and MDI teams for providing the wonderful data. We also would like to thank the BBSO and Observatoires de Paris teams for observing the data. SOHO is a project of international cooperation between ESA and NASA.

References

- Berdichevsky D., Bougeret J.-L., Delaboudinière J-P. et al., 1998, *Geophys. Res. Lett.*, 25, 2473
- Bray R. J., Cram L. E., Durrant C. J., and Loughhead R. E., 1991, *Plasma Loops in the Solar Corona*, Cambridge Astrophysics Series 18, Cambridge: Cambridge University Press
- Brueckner G. E., Howard R. A., Koomen M. J. et al., 1995, *Solar Phys.*, 162, 357
- Bruzek A., 1964, *ApJ*, 140, 746
- Carmichael H., 1964, In: W. N. Hess, ed., *AAS-NASA Symposium on Physics of Solar Flares*, NASA SP-50, p. 451
- Choudhary D. P., Gary G. A., 1999, *Solar Phys.*, 188, 345
- Delaboudinière J-P., Artzner G. E., Brunaud J. et al., 1995, *Solar Phys.*, 162, 291
- Dere K. P., Brueckner G. E., Howard R. A. et al., 1997, *Solar Phys.*, 175, 601
- Engvold O., 1989, In: E. R. Priest, ed., *Dynamics and Structure of Quiescent Solar Prominences*, Academic Publishers, Holland: Dordrecht, p. 47
- Forbes T. G., Malherbe J. M., Priest E. R., 1989, *Solar Phys.*, 120, 285
- Forbes T. G., Acton L. W., 1996, *ApJ*, 459, 330
- Gosling J. T., 1997, In: N. Crooker, J. A. Joselyn, and J. Feynman, eds., *Coronal Mass Ejections*, AGU Geophysical Monograph 99, p.9
- Hirayama T., 1974, *Solar Phys.*, 34, 323
- Hori K., Yokoyama T., Kosugi T., Shibata K., 1998, *ApJ*, 500, 492
- Howard R. A., Michels D. J., Sheeley N. R., Koomen M. J., 1982, *ApJ*, 263, L101
- Hundhausen A. J., 1997, In: N. Crooker, J. A. Joselyn, and J. Feynman, eds., *Coronal Mass Ejections*, AGU Geophysical Monograph 99, p.7
- Illing R. M., Hundhausen A. J., 1985, *J. Geophys. Res.*, 90, 275
- Kopp R. A., Pneuman G. W., 1976, *Solar Phys.*, 50, 85
- Low B. C., 1992, *ApJ*, 399, 300
- Martin S. F., Livi S. H. B., 1992, In: Z. Švestka, B. V. Jackson and M. E. Machado, eds., *Lecture Notes in Physics*, Berlin: Springer-Verlag, 399, 33
- McAllister A. H., Dryer M., McIntosh P., Singer H., Weiss L., 1996, *J. Geophys. Res.*, 101, 13498
- Plunkett S. P., Thompson B. J., Howard R. A. et al., 1998, *Geophys. Res. Lett.*, 25, 2477
- Scherrer P. H., Bogart R. S., Bush R. I. et al., 1995, *Solar Phys.*, 162, 129
- Sturrock P. A., 1966, *Nature*, 211, 695
- Švestka Z. F., Fontenla J. M., Mackado M. E., Martin S.F., Neidig D. F., 1987, *Solar Phys.*, 108, 237
- Švestka Z., Cliver E. W., 1992, In: Z. Švestka, B. V. Jackson, and M. E. Machado, eds., *Lecture Notes in Physics* 399, 1
- Thompson B. J., Plunkett S. P., Gurman J. B., Newmark J. S., St. Cyr O. C., Michels D. J., 1998, *Geophys. Res. Lett.*, 25, 2461
- Van Ballegooijen A. A., Martens P. C. H., 1989, *ApJ*, 343, 971
- Wang J., Shi Z., 1993, *Solar Phys.*, 143, 119
- Wang J., Shi Z., Martin S. F., 1996, *A&A*, 316, 201
- Wang J., 2001, *Space Sci. Rev.*, 95, 55
- Zhang J., Wang J., 2000, *Geophys. Res. Lett.*, 27, 2877
- Zhang J., Wang J., 2001, *ApJ*, in press
- Zhang J., Wang J., Deng Y., Wu D., 2001, *ApJ*, 548, L99
- Zirin H., 1986, *Astrophysics of the Sun*, Camb. Univ. Press